Collective enhancements in the level densities of Dy and Mo isotopes

A. Rahmatinejad,[1] T. M. Shneidman,[1,*] N. V. Antonenko,[1,2,†] A. N. Bezbakh,[1] G. G. Adamian,[1] and L. A. Malov[1]
[1]*Joint Institute for Nuclear Research, Dubna 141980, Russia*
[2]*Tomsk Polytechnic University, Tomsk 634050, Russia*

(Received 2 February 2020; accepted 11 May 2020; published 27 May 2020)

Nuclear level densities in ^{94,96,98}Mo and ^{160,162,164}Dy isotopes are calculated using the single-particle spectrum obtained with the Woods-Saxon potential. The level-density parameters, spin cut-off factors, and moments of inertia are studied. Using the available experimental data at low excitation energies, the collective enhancements of the level densities are calculated and compared with those of the phenomenological model. In Mo isotopes, these semiempirical calculations agree better with the experiments in comparison to the phenomenological model assuming a spherical shape.

DOI: 10.1103/PhysRevC.101.054315

I. INTRODUCTION

Nuclear level density is of crucial importance in the calculation of cross sections and survival probabilities in fusion and fission reactions. There are several methods for the calculation of nuclear level densities which are mainly based on two, combinatorial and thermodynamical, approaches. The combinatorial models are built either on nuclear mean-field theory [1,2] or beyond mean-field methods which take into account the effective nucleon-nucleon interactions [3,4] and can provide exact level densities as a function of excitation energy, spin, and parity. A recently developed combinatorial method has been used to study pairing gaps, parity, and angular-momentum distribution of nuclear level densities and nuclear shape evolution [5,6]. The combinatorial models require large scale computations to estimate the number of ways in which the nucleons can be distributed among the available single-particle levels.

The thermodynamical models which are based on the partition-function method provide simpler formulas for the nuclear level density. The analytical expression of the Fermi-gas model, proposed in the thermodynamical approach, is widely used to calculate the level densities [7]. Although this approach is not so sophisticated, it is convenient to use in many applications of the level density. For the nuclei lighter than Cf, the systematic studies of the free parameters in the Fermi-gas model and a good compilation of the experimental data are given in Refs. [8,9]. By treating the pairing and shell effects in the frame of superfluid formalism [10,11], one can keep the simplicity of the Fermi-gas model for more realistic studies. This method was used to study the level densities of superheavy nuclei and dinuclear systems [12,13].

Previously, the experimental data on the level density were limited to near stable nuclei and very low energies where the information about low-lying discrete levels and neutron resonance spacing is accessible. Recently, new methods mainly developed by the Oslo group [14,15] provide experimental data in a wide range of excitation energy and angular momentum. Experimental level densities of Dy and Mo isotopes were determined up to neutron separation energy [16–21].

Dysprosium isotopes in the rare earth region are well-deformed and hence of interest for the study of collective effects. Molybdenum isotopes are in the transitional region. This mass region is characterized by a competition between different shapes or low-lying configurations based on different intrinsic deformations, that leads to the shape coexistence phenomena [22]. Therefore, the study of shapes and collective excitations in this region provides important insights on nuclear structure. The structure studies of shape coexistence in molybdenum isotopes have recently received considerable attention [23–25].

To compare the calculated level densities with the experimental data, the collective effects should be taken into account. There is a phenomenological expression introduced by Ignatyuk [26] for the collective effects in the form of a product of vibrational and rotational coefficients. This expression is not appropriate for soft or transitional nuclei. For an ideal spherical nucleus with a rotational symmetry, only vibrational collective excitations are expected. However, in the case of a deformed nucleus, the rotational excitations can be observed. One of the experimental indications of deformation in a nucleus is the ratio of the energy of the first 4^+ state to that of the first 2^+ state, known as the $R_{4/2}$ ratio [27]. Generally, a nucleus with $R_{4/2} \approx 3.33$ is considered as a rotor with a rigid-body moment of inertia. For instance, $R_{4/2} = 3.27$, 3.29, and 3.3 in ^{160}Dy, ^{162}Dy, and ^{164}Dy isotopes, respectively [28–30]. Therefore, Dy can be considered as a rigid rotor in the calculation of collective effects.

After spherical ^{92}Mo with a neutron shell closure, the shape of molybdenum isotopes starts to change with increasing mass number. In ^{94}Mo, ^{96}Mo, and ^{98}Mo isotopes, $R_{4/2} \approx$ 1.8–2 [31–33]. At energies less than pair-breaking all the experimentally observed excitations can be considered as collective states. In the microscopic calculations, the rotational and vibrational bands of the deformed nucleus are in good

*Also at Kazan Federal University, Kazan 420008, Russia.
†antonenk@theor.jinr.ru

TABLE I. Calculated values of deformation parameters β_2 and β_4, shell corrections $\delta E_{\rm sh}$, pairing energies $E_{\rm pair}$, and neutron Δ_n and proton Δ_p pairing gaps in the ground state of nuclei are indicated. The deformation parameters and shell corrections are compared with those from Ref. [47].

Nucleus	β_2	β_4	$\delta E_{\rm sh}$ (MeV)	β_2 [47]	β_4 [47]	$\delta E_{\rm sh}$ (MeV) [47]	Δ (MeV)	$E_{\rm pair}$ (MeV)
^{160}Dy	0.284	0.045	−1.2677	0.272	0.053	−2.30	$\Delta_n = 1.06$	2.19
							$\Delta_p = 1.31$	
^{162}Dy	0.311	0.050	−2.2766	0.283	0.044	−2.88	$\Delta_n = 0.96$	1.89
							$\Delta_p = 1.26$	
^{164}Dy	0.313	0.048	−2.9060	0.296	0.022	−3.47	$\Delta_n = 0.97$	1.65
							$\Delta_p = 1.22$	
^{94}Mo	0.080	0.015	−2.8055	0.000	0.000	−1.24	$\Delta_n = 1.15$	3.82
							$\Delta_p = 1.80$	
^{96}Mo	0.072	0.007	−0.5434	0.150	0.045	0.17	$\Delta_n = 1.17$	3.96
							$\Delta_p = 1.79$	
^{98}Mo	0.035	0.013	1.3024	0.206	0.017	0.86	$\Delta_n = 1.36$	4.02
	0.196	0.023	1.0082				$\Delta_p = 1.65$	3.21

agreement with the experimental data [34–38]. However, in the case of transitional nuclei there is a discrepancy between the calculated collective excitations and those obtained from the experimental data [22]. In Ref. [5], using a combinatorial model for the nuclear level density, the role of collective enhancements has been investigated in several deformed, transitional, and spherical nuclei. As shown, an account of rotational excitations results in fairly good agreement with the experiments for almost spherical ^{97,98}Mo isotopes.

In this work, we use the Woods-Saxon single-particle spectrum in the superfluid model to calculate intrinsic nuclear level densities for Dy and Mo nuclei. Taking into account pairing and shell-correction effects, the energy dependence of the level density parameter and spin cut-off factor are investigated. Based on the available experimental data [28–33], the semiempirical calculation of collective effects is proposed. The validity of the macroscopic expression of collective enhancements [26] is especially examined for the transitional Mo isotopes.

In Sec. II, the superfluid formalism is briefly outlined. Energy dependences of the nuclear level density parameter and spin cut-off factor are studied in Secs. III and IV, respectively. The calculation of collective enhancements in the macroscopic approach and from the available experimental data is presented in Sec. V for deformed and spherical nuclei. The results of calculations are compared with the experimental data [17–21] in Sec. VI.

II. INTRINSIC LEVEL DENSITY

Considering the nucleus as a system of independent quasiparticles, the logarithm of the grand partition function is written as [10,11,39]

$$\Omega = -\beta \sum_{\tau=p,n} \left[\sum_k (\varepsilon_{\tau k} - \lambda_\tau - E_{\tau k}) + 2 \sum_k \log[1 + \exp(-\beta E_{\tau k})] - \beta \frac{\Delta_\tau^2}{G_\tau} \right], \quad (1)$$

where λ_τ and Δ_τ are chemical potentials and pairing gap parameters for neutron ($\tau = n$) and proton ($\tau = p$) subsystems, respectively. The inverse temperature is denoted by $\beta = 1/T$. In Eq. (1), thermal equilibrium is assumed between neutron and proton subsystems.

The single-particle energies $\varepsilon_{\tau k}$ and the corresponding quasiparticle energies $E_{\tau k} = \sqrt{(\varepsilon_{\tau k} - \lambda_\tau)^2 + \Delta_\tau^2}$ are calculated within the quasiparticle-phonon model (QPM) [40,41] with the mean-field potential in the Woods-Saxon form. The pairing correlations are evaluated with the BCS approach. The monopole pairing strength constants G_τ were adjusted to reproduce the odd-even difference of experimental ground-state nuclear masses [42,43]

$$\Delta_n(N,Z) = -\tfrac{1}{2}[B(N-1,Z) + B(N+1,Z) - 2B(N,Z)],$$
$$\Delta_p(N,Z) = -\tfrac{1}{2}[B(N,Z-1) + B(N,Z+1) - 2B(N,Z)], \quad (2)$$

where B's are the binding energies of the corresponding nuclei. As in Refs. [44,45], the calculated shell corrections were incorporated into the macroscopic-microscopic approach [46] to define the equilibrium deformations.

In Table I, the calculated quadrupole β_2 and hexadecapole β_4 deformations, shell corrections $\delta E_{\rm sh}$, and neutron Δ_n and proton Δ_p pairing gaps are presented for ^{160,162,164}Dy and ^{94,96,98}Mo nuclei. As seen, the values of β_2 and β_4 are close to those calculated in Ref. [47]. Dysprosium isotopes are strongly deformed with quadrupole deformation parameters larger than 0.2. The shapes of molybdenum isotopes are changing from spherical to deformed with increasing mass number. In the case of ^{98}Mo, our calculations yield two minima characterized by different deformations but similar values of shell corrections. In this case, a shape coexistence or deformed shape even at low excitation energies is expected in agreement with the experimental observations [23,24]. In the calculations of the deformed state the pairing constants were taken from the nearly spherical results.

Assuming the nucleus in a thermal equilibrium state, the BCS equations, which determine the temperature dependence

TABLE II. The values of adjustable parameters in Eq. (11) for the level density parameter, calculated critical temperatures (T_{cn} for neutron and T_{cp} for proton) and corresponding critical energies for ^{160,162,164}Dy and ^{94,96,98}Mo nuclei. The rigid-body $\Im_{r.b.}$ and experimental $\Im_{\rm exp} = 3/E_{2^+}$ moments of inertia adjusted to reproduce the energy of lowest 2^+ states taken from [28–33].

Nucleus	$\tilde{a}'$ (MeV^{-1})	E'_{D1} (MeV)	E'_{D2} (MeV)	$T_{\rm cr}$ (MeV)	$U_{\rm cr}$ (MeV)	$\Im_{r.b.}$ ($\hbar^2$/MeV)	$\Im_{\rm exp}$ ($\hbar^2$/MeV)
^{160}Dy	13.40	2.22	4.30	$T_{cn} = 0.60$ $T_{cp} = 0.77$	10.44	65.46	34.56
^{162}Dy	13.58	10.35	2.24	$T_{cn} = 0.56$ $T_{cp} = 0.74$	9.30	66.83	37.19
^{164}Dy	13.77	10.71	2.04	$T_{cn} = 0.56$ $T_{cp} = 0.71$	8.58	68.21	40.87
^{94}Mo	8.82	2.89	29.33	$T_{cn} = 0.70$ $T_{cp} = 0.99$	10.93	26.98	3.44
^{96}Mo	9.23	0.42	6.82	$T_{cn} = 0.70$ $T_{cp} = 0.98$	12.08	27.94	3.85
^{98}Mo	9.38	7.84 ($\beta_2 = 0.035$) 10.85 ($\beta_2 = 0.196$)	2.96 2.49	$T_{cn} = 0.81$ $T_{cp} = 0.91$ $T_{cn} = 0.69$ $T_{cp} = 0.92$	12.46 11.31	28.92	4.08

of Δ_τ and λ_τ, are derived from Eq. (1):

$$\frac{2}{G_\tau} = \sum_k \frac{1}{E_{\tau k}} \tanh \frac{\beta E_{\tau k}}{2},$$
$$N_\tau = \sum_k \left(1 - \frac{\varepsilon_{\tau k} - \lambda_\tau}{E_{\tau k}} \tanh \frac{\beta E_{\tau k}}{2}\right), \tag{3}$$

where $N_p = Z$ and $N_n = N$. Equations (3) must be valid at each value of β. The calculated pairing gap is a decreasing function of temperature. It reaches $\Delta = 0$ at critical temperature $T_{\rm cr}$. The values of $T_{\rm cr}$ obtained for the considered nuclei are presented in Table II. The corresponding excitation energies are about $U_{\rm cr} = 10$ MeV for Dy isotopes, and $U_{\rm cr} = 12$ MeV for Mo isotopes (see Table II).

The excitation energy $U = U_n + U_p$ is calculated as

$$E_\tau(T) = \sum_k \varepsilon_{\tau k}\left(1 - \frac{\varepsilon_{\tau k} - \lambda_\tau}{E_{\tau k}} \tanh \frac{\beta E_{\tau k}}{2}\right) - \frac{\Delta_\tau^2}{G_\tau},$$
$$U_\tau(T) = E_\tau(T) - E_\tau(0), \tag{4}$$

and entropy $S = S_n + S_p$,

$$S_\tau(T) = 2\sum_k \left\{\log[1 + \exp(-\beta E_{\tau k})] + \frac{\beta E_{\tau k}}{1 + \exp(\beta E_{\tau k})}\right\}. \tag{5}$$

Then, employing the saddle point method [10], the intrinsic level density ρ_i is obtained as

$$\rho_i = \frac{\exp(S)}{(2\pi)^{\frac{3}{2}}\sqrt{D}}, \tag{6}$$

where D is the determinant of the matrix comprised of the second derivatives of entropy with respect to β and $\mu_\tau = \beta\lambda_\tau$ at saddle point:

$$D = \begin{vmatrix} \frac{\partial^2 S}{\partial \beta^2} & \frac{\partial^2 S}{\partial \beta \partial \mu_p} & \frac{\partial^2 S}{\partial \beta \partial \mu_n} \\ \frac{\partial^2 S}{\partial \beta \partial \mu_p} & \frac{\partial^2 S}{\partial \mu_p^2} & 0 \\ \frac{\partial^2 S}{\partial \beta \partial \mu_n} & 0 & \frac{\partial^2 S}{\partial \mu_n^2} \end{vmatrix}. \tag{7}$$

From the assumption of thermal equilibrium between neutron and proton subsystems we obtain $\partial S^2/\partial\mu_n\partial\mu_p = 0$.

The intrinsic level densities calculated for ^{160,162,164}Dy and ^{94,96,98}Mo isotopes are displayed in Figs. 1 and 2, respectively. A comparison between the intrinsic level density of ^{98}Mo calculated with an almost spherical level scheme and the one calculated with the deformed level scheme is displayed in panel (c) of Fig. 2. As both spectra are obtained for

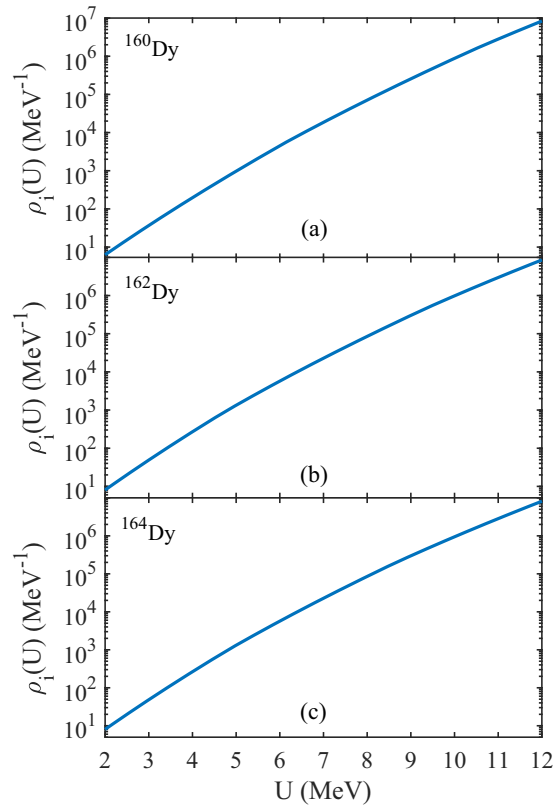

FIG. 1. Calculated energy dependent intrinsic level densities in ^{160}Dy, ^{162}Dy, and ^{164}Dy.

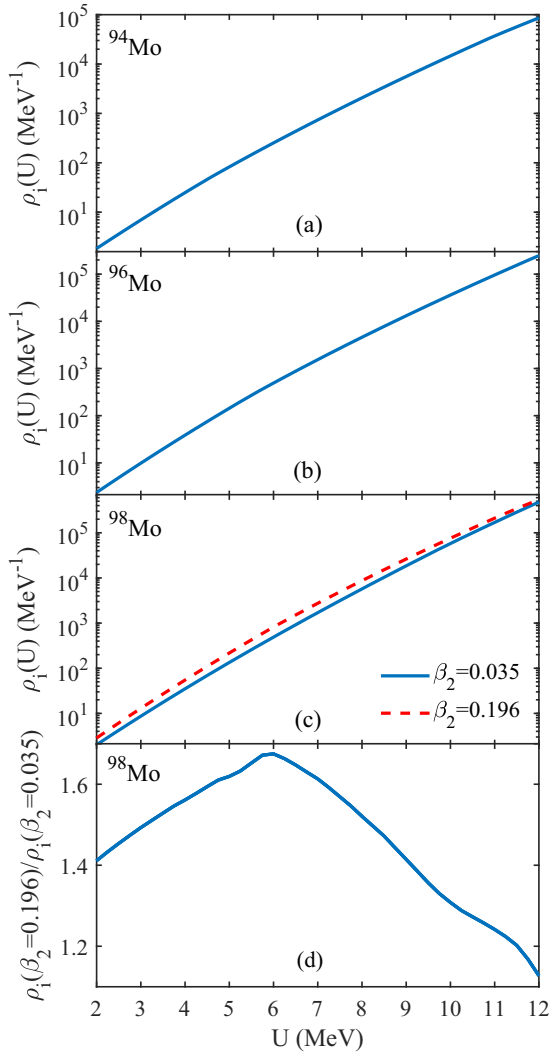

FIG. 2. Calculated intrinsic level densities in ^{94}Mo, ^{96}Mo, and ^{98}Mo. The dashed line (c) is obtained with the single-particle energies in the deformed state. The ratio of intrinsic level densities obtained with the single-particle spectra at the deformed and almost spherical states is shown (d).

close minima of the potential energy surface and the shell corrections (see Table I) and the single-particle level densities near the Fermi surface are similar, the close values of intrinsic level densities are expected. Indeed, due to different dampings of shell and pairing effects, the ratio of intrinsic level densities at deformed and spherical states is about 1.2–1.6 at low excitation energies [Fig. 2(d)].

III. LEVEL-DENSITY PARAMETER

In many applications, one can use the Fermi-gas prescription of the level density [48]. For example, it is often used in the phenomenological calculations of the survival probabilities of excited nuclei [8,9]. In the case of the Fermi-gas model, the connection between the nuclear temperature and excitation energy is established by the level-density parameter a as

$$U = aT^2. \tag{8}$$

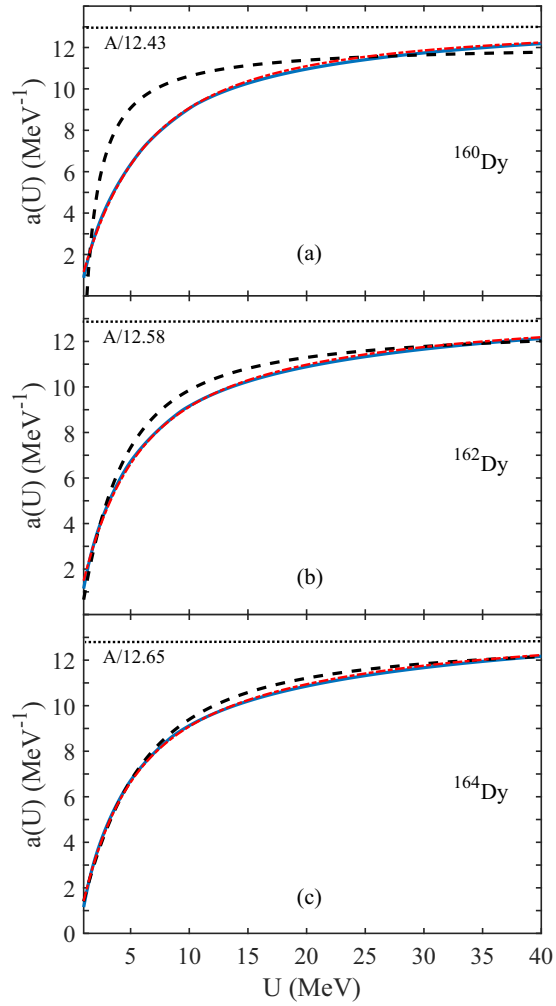

FIG. 3. Calculated energy dependent level density parameters in ^{160}Dy, ^{162}Dy, and ^{164}Dy (blue solid lines) are compared with the phenomenological expression (10) without (black dashed lines) and with (red dash-dotted lines) pairing effect. The dotted lines indicate the asymptotic values of the calculated level-density parameters.

To keep the simplicity of the Fermi-gas model in realistic calculations, one can introduce the energy dependence of the level density parameter. For that, the microscopic level density ρ_i can be fitted with the Fermi-gas expression

$$\rho_{FG} = \frac{\sqrt{\pi}}{12[a(U)]^{1/4}U^{5/4}} \exp\left(2\sqrt{a(U)U}\right). \tag{9}$$

The results obtained for ^{160,162,164}Dy and ^{94,96,98}Mo nuclei are presented in Figs. 3 and 4, respectively. As seen, $a(U)$ increases with excitation energy and gradually reaches an asymptotic value $\tilde{a}$ (see Table II). Assuming a linear dependence of the level-density parameter on the mass number, we have $\tilde{a} \approx A/(12.4\text{–}12.6)$ MeV^{-1} for Dy isotopes, and $\tilde{a} \approx A/(10.3\text{–}11.0)$ MeV^{-1} for Mo isotopes. These results are consistent with the average value $a \approx A/(8\text{–}13.5)$ estimated in [49]. Note that in the model presented, the evolution of deformation with excitation energy is not taken into account. Therefore, as seen in Fig. 4(c), at higher energies ($U > 10$

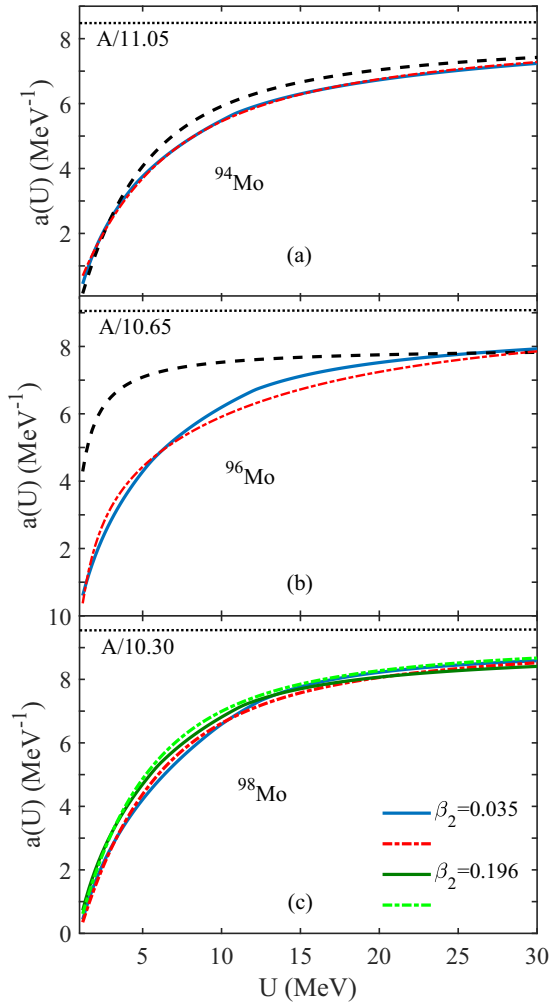

FIG. 4. The same as in Fig. 3, but for ^{94}Mo, ^{96}Mo, and ^{98}Mo. The microscopic calculations (blue solid lines) are compared with the phenomenological expression (10) without (black dashed lines) and with (red dash-dotted lines) pairing effect. The green curves in (c) are the calculations (solid line) with the single-particle energies in the deformed state and the corresponding results of Eq. (11) (dashed line). The dotted lines indicate the asymptotic values of the calculated level density parameters.

MeV) the level-density parameters calculated for ^{98}Mo with the single-particle energies in almost spherical and deformed states are slightly different.

The energy dependence of the level-density parameter can be explained by the damping of the shell correction with the excitation energy and described by the phenomenological function [50]

$$a(U) = \tilde{a}\left[1 + \frac{1 - \exp\left(-U/E_D\right)}{U}\delta E_{\rm sh}\right], \qquad (10)$$

where E_D is the damping parameter which is adjusted along with $\tilde{a}$ to reproduce the microscopic calculations.

The results obtained with Eq. (10) are shown in Figs. 3 and 4. As seen, the phenomenological expression does not describe well the behavior of $a(U)$ for the isotopes with $|\delta E_{\rm sh}| < 1.5$ MeV. Moreover, in the case of ^{98}Mo which has a positive shell correction, the microscopic results cannot be fitted with Eq. (10). For the cases of small or positive shell corrections, the phenomenological expression (10) is modified by taking into account the damping of pairing effects

$$a(U) = \tilde{a}'\left[1 + \frac{1 - \exp\left(-U/E'_{D1}\right)}{U}\delta E_{\rm sh} - \frac{1 - \exp\left(-U/E'_{D2}\right)}{U}E_{\rm pair}\right]. \qquad (11)$$

Here, $E_{\rm pair}$ is the pairing energy. For the isotopes considered, the calculated $E_{\rm pair}$ values are presented in Table I. The values of adjustable parameters in Eq. (11) are presented in Table II. As shown in Figs. 3 and 4, the account of the damping of pairing effects results in a good agreement with the microscopic results.

IV. SPIN CUT-OFF PARAMETER

Spin cut-off parameter σ^2 determining the level density spin distribution is calculated as [51]

$$\sigma^2 = \frac{1}{2}\sum_{\tau=p,n}\sum_{k} m_{\tau k}^2 \cosh^{-2}\left(1/2\beta E_{\tau k}\right), \qquad (12)$$

where $m_{\tau k}$ are the single-particle spin projections. The calculated energy dependencies of σ^2 for Dy and Mo isotopes are shown in Fig. 5. As seen, σ^2 depends almost linearly on excitation energy for all nuclei considered. However, at the energy around 6–8 MeV the slopes of the curves change. This change is more evident for Mo isotopes while for Dy it is smeared out. Such a behavior is related to the phase transition from the superfluid to normal phase. As seen from Table II, the slopes of the curves change in the vicinity of the critical excitation energy.

As shown in [52], the spin cut-off parameter is related to the effective moment of inertia

$$\Im = \frac{\hbar^2\sigma^2}{T}. \qquad (13)$$

The energy dependencies of σ^2/T for Dy and Mo isotopes are displayed in Fig. 6. As expected, the σ^2/T which is equivalent to the moment of inertia increases quickly at the energy range from $U = 5$ MeV to $U = 15$ MeV and stays almost constant afterwards. At high excitation energy, where the pairing is damped out, the nuclear moment of inertia reaches the rigid body value $\Im_{r.b.}$, while at lower excitations it can be estimated from the energy of the lowest 2^+ state as $\Im_{\rm exp} = 3/E_{2^+}$ (see Table II). It is interesting that in Mo isotopes despite their almost spherical equilibrium shape (see Table I) the moments of inertia quickly approach their asymptotic values at $U > U_{\rm cr}$. Therefore, in the calculation of total level density the rotational enhancement cannot be excluded (see Sec. V).

V. COLLECTIVE ENHANCEMENTS

The total level density, which includes collective states, must be calculated to be compared with the experimental data. With the assumption of a decoupling between intrinsic and collective degrees of freedom, the excitation energy of a

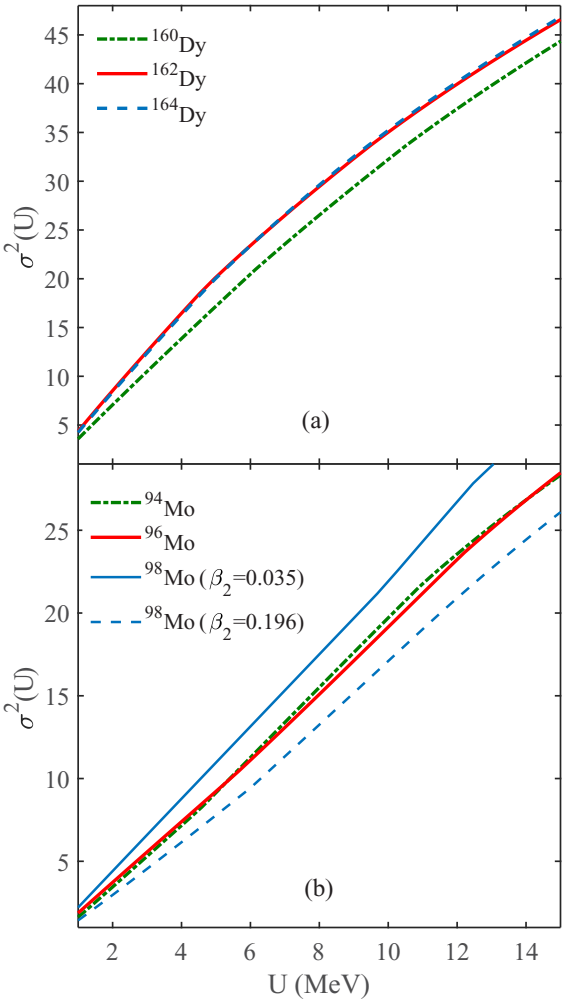

FIG. 5. Energy dependence of the spin cut-off parameters for ^{160,162,164}Dy (a) and ^{94,96,98}Mo (b) calculated with the microscopic expression (12).

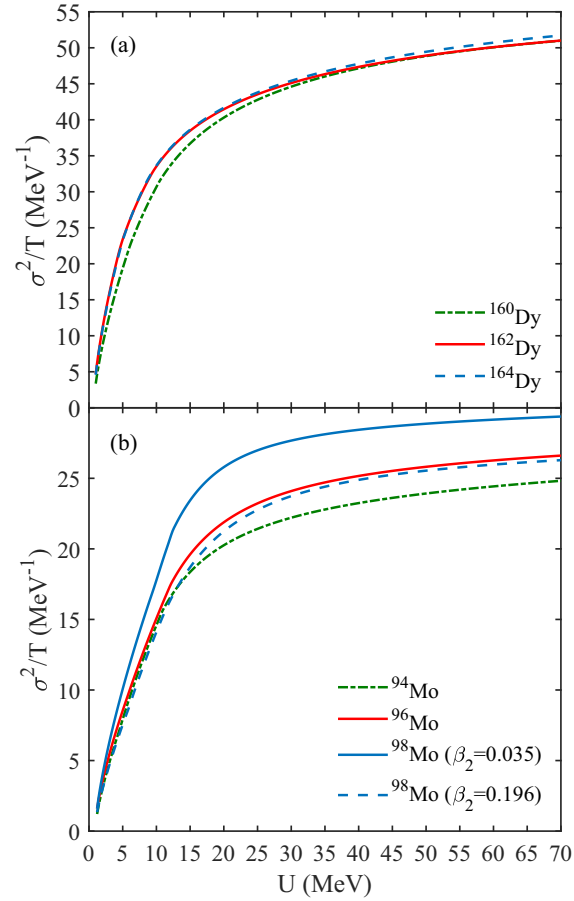

FIG. 6. Energy dependence of σ^2/T in ^{160,162,164}Dy (a) and ^{94,96,98}Mo (b).

nucleus can be written as a sum of intrinsic U_i and collective U_c excitation energies $U = U_i + U_c$. The total level density is then written as

$$\rho_{\rm tot}(U) = \int \rho_i(U_i)\rho_{\rm coll}(U - U_i)dU_i, \tag{14}$$

where the collective level density is

$$\rho_{\rm coll}(U - U_i) = \sum_c \delta(U - U_i - U_c)\tau_c(U_c). \tag{15}$$

The degeneracy of a collective state with the angular momentum I_c is $\tau_c(U_c) = 2I_c + 1$. Using Eq. (15), we obtain

$$\rho_{\rm tot}(U) = \sum_c \rho_i(U - U_c)\tau_c(U_c). \tag{16}$$

The energies U_c can either be taken from the experiment or calculated using a collective model. Assuming that the most important collective modes are the quadrupole and octupole vibrations, the spectrum of collective excitations in deformed nucleus is given as

$$U_c = \hbar\omega_\beta(n_\beta + 1/2) + \hbar\omega_\gamma(2n_\gamma + |K|/2 + 1) + \frac{\hbar^2}{2\Im}[I_c(I_c + 1) - K^2], \tag{17}$$

where K is the projection of I_c on the symmetry axis, and n_β and n_γ are the quantum numbers of harmonic oscillator energies. Since the octupole deformation stabilizes with angular momentum [53] we can assume for simplicity that the nucleus has stable octupole deformation and each state with $K \neq 0$ is twofold degenerate $\tau_c(U_c) = 2(2I_c + 1)$. For $K = 0$, the octupole deformation leads to the appearance of 1^-, 3^-, 5^-,... excitations, which again can be approximately taken into account by factor 2 in $\tau_c(U_c)$. The values of $\hbar\omega_\beta$ and $\hbar\omega_\gamma$ in Eq. (17) are taken to reproduce the experimental data on the lowest 0^+ and 2^+ band heads [28–33]. The moments of inertia are taken as $\Im = \Im_{\rm exp}$ (see Table II). The number of collective levels calculated with Eq. (17) for ^{164}Dy is displayed as a function of excitation energy in Fig. 7(a). As seen, the calculations are in a good agreement with the available experimental data at low energies [30]. The values of $\hbar\omega_\beta$ and $\hbar\omega_\gamma$ are taken as 1.27 MeV and 0.74 MeV, respectively. Since the lowest 0^+ band is most likely not a β vibrational band head the value of $\hbar\omega_\beta$ is taken as for ^{160}Dy.

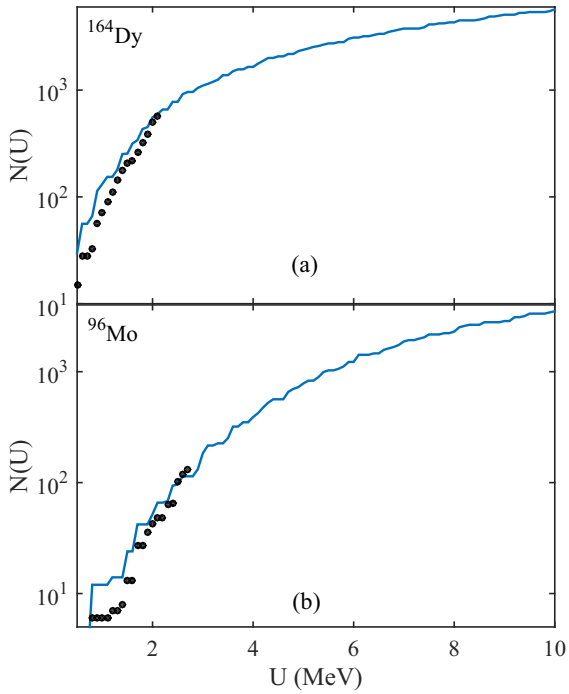

FIG. 7. (a) The number of collective levels in ^{164}Dy calculated with the semiempirical expression (solid line) as a function of excitation energy, in comparison with the available experimental data at low energies (symbols) [30]. (b) The same as (a), but for ^{96}Mo. The experimental data are taken from [32].

Similar calculation for ^{96}Mo is presented in Fig. 7(b). In this case, $\hbar\omega_\beta = 1.15$ MeV and $\hbar\omega_\gamma = 1.24$ MeV. On the contrary to Dy isotopes, the ground-state band calculated with the moment of inertia $\Im_{\rm exp}$ is not in good agreement with the experimental data at low energies in Mo isotopes [31,32]. Our calculations show that at low energies, the moment of inertia is not constant but depends on I values. We found that the moments of inertia of the yrast bands in ^{94,96}Mo can be fitted with the following expression:

$$\Im = \Im_{r.b}\big(1 - a_1 \exp[-a_2 I(I+1)]\big), \tag{18}$$

where the parameters are $a_1 = 0.89$ and $a_2 = 0.006$. The moments of inertia obtained give a good agreement with the asymptotic values of the σ^2/T curves displayed in Fig. 6 at large values of I. As seen from Fig. 7(b), the calculations are in good agreement with the available experimental data at low energies [32].

Alternative way to take into account the collective enhancement of nuclear level density is to use an adiabatic approximation [26]

$$\rho_{\rm tot}(U) = \rho_i(U) K_{\rm coll}, \tag{19}$$

where

$$K_{\rm coll} = K_{\rm rot} K_{vib}. \tag{20}$$

The enhancement due to rotational degrees of freedom is expressed as [8,26]

$$K_{\rm rot} = \begin{cases} 1, & \text{for spherical nuclei} \\ \Im_\perp T, & \text{for deformed nuclei,} \end{cases} \tag{21}$$

where $\Im_\perp = \Im_{r.b} f(\beta_2, \beta_4)$ is the moment of inertia with respect to the axis perpendicular to the symmetry axis. Here,

$$f(\beta_2, \beta_4) = 1 + \sqrt{5/16\pi}\,\beta_2 + (45/28\pi)\beta_2^2 + (15/7\pi\sqrt{5}\beta_2\beta_4), \tag{22}$$

where β_2 and β_4 are quadrupole and hexadecapole deformation parameters of the nucleus. The liquid-drop model estimation for the vibrational enhancement [8,26] is

$$K_{\rm vib} = \exp(0.0555 A^{2/3} T^{4/3}). \tag{23}$$

The collective enhancement $K_{\rm coll}$ can also be obtained from the experimental data or from Eq. (17). Expanding the right-hand side of Eq. (16) to the first order in U_c at $U \gg U_c$ [54], we obtain

$$\begin{aligned} \rho_{\rm tot}(U) &\simeq \sum_c \left[\rho_i(U) - U_c \frac{\partial \rho_i(U)}{\partial U}\right]\tau_c(U_c) \\ &= \sum_c \left[\rho_i(U) - \frac{U_c}{T}\rho_i(U)\right]\tau_c(U_c). \end{aligned} \tag{24}$$

Here, we use $\frac{\partial \rho(U)}{\partial U} = \frac{\rho(U)}{T}$. One can calculate this derivative using the Fermi-gas expression (9), taking into account the energy dependence of the level density parameter. Equation (24) is considered as the Taylor expansion of the following expression:

$$\rho_{\rm tot}(U) \simeq \rho_i(U) \sum_c \exp\left(-\frac{U_c}{T}\right)\tau_c(U_c), \tag{25}$$

to the first order of U_c/T [54]. Based on Eq. (25), the vibrational-rotational collective enhancement is obtained as

$$K_{\rm coll} = \sum_c \exp\left(-\frac{U_c}{T}\right)\tau_c(U_c). \tag{26}$$

The comparison between the collective enhancement factors calculated with Eqs. (20)–(23) and Eq. (26) is presented in Fig. 8 for Dy isotopes. In the approach presented in this paper, only quadrupole and octupole vibrational degrees of freedom are taken into account. However, in the macroscopic approach [26] the vibrational excitations of higher multipolarities are also counted. Therefore, at low energies, where only quadrupole and octupole excitations can be excited, the results of two approaches are close to each other. At higher energies after damping of pairing, where the intrinsic and collective excitations are mixed, the assumption of all higher orders collective effects in the macroscopic approach leads to an overestimation of the collective enhancement. Therefore, the difference between two approaches increases with excitation energy.

In the macroscopic expression of collective enhancements in spherical nuclei, the rotational coefficient is taken as unity. This is applicable if the nucleus is assumed to be ideally spherical. In order to examine validity of this assumption for

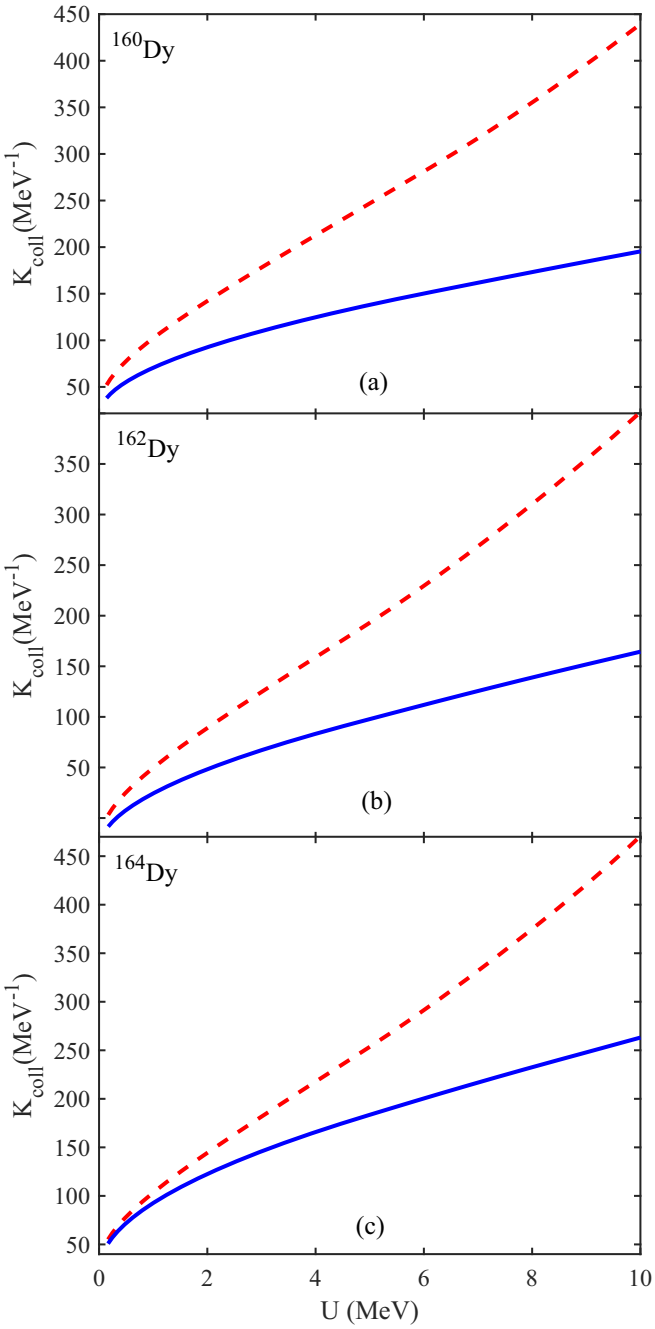

FIG. 8. Calculated collective enhancement factors with Eqs. (20)–(23) (red dashed lines) and Eq. (26) (blue solid lines) for ^{160,162,164}Dy.

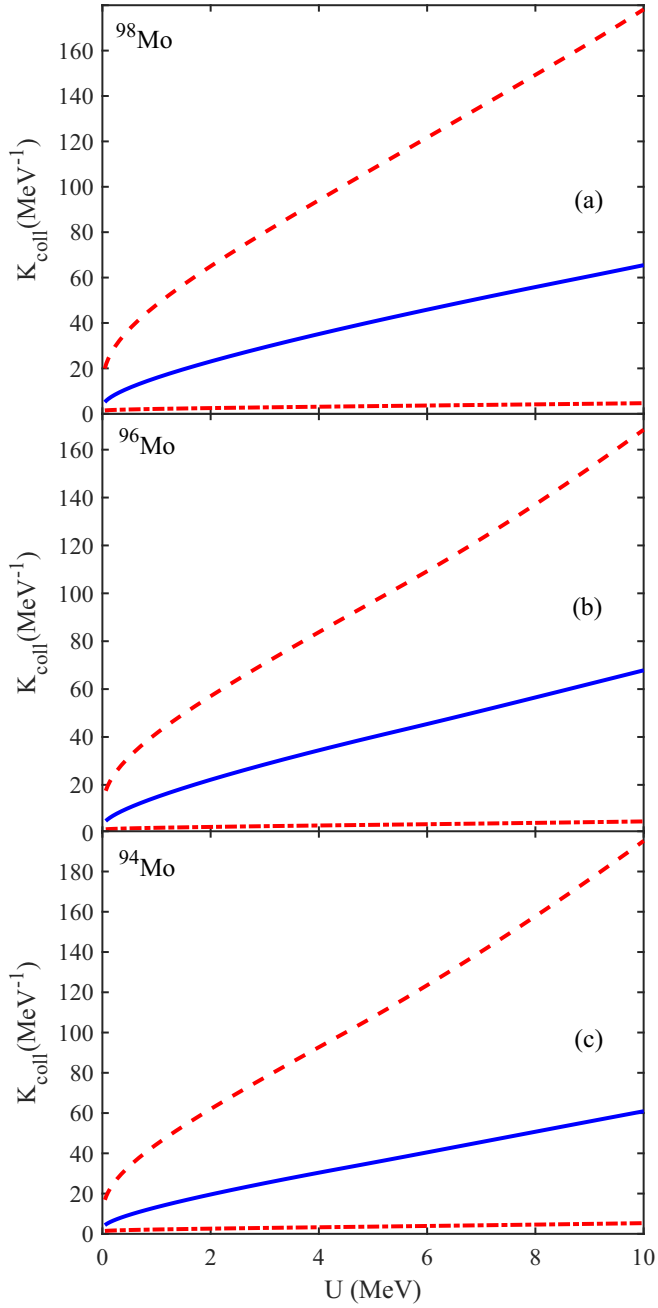

FIG. 9. Collective enhancement factors calculated with Eqs. (20)–(23) with $K_{\rm rot}$(red dashed lines) and without $K_{\rm rot}$ (red dash-dotted lines) are compared with those from Eq. (26) (blue solid lines) for ^{94,96,98}Mo.

Mo isotopes, we calculated the collective enhancements with the semiempirical expression (26). The results are shown in Fig. 9 for ^{94,96,98}Mo isotopes. For ^{98}Mo, the values of a_1 and a_2 in Eq. (18) are taken as the same for ^{94}Mo and ^{96}Mo because of the lack of data. As seen, taking into account only the vibrational coefficient for Mo isotopes, we underestimate the collective enhancement factors. This result is consistent with the behavior of effective moment of inertia which sharply increases to the rigid-body value at critical excitation energy [see Fig. 7(b)].

VI. COMPARISON WITH EXPERIMENTS

Taking into account the average spin distribution of the levels, the nuclear level density $\rho(U)$ is calculated as

$$\rho(U) = \frac{\rho_{\rm tot}(U)}{\sqrt{2\pi\sigma^2}}. \tag{27}$$

The results are presented in Fig. 10 for ^{162,164}Dy together with the corresponding experimental data [17–19]. The total level density was calculated with the collective enhancement

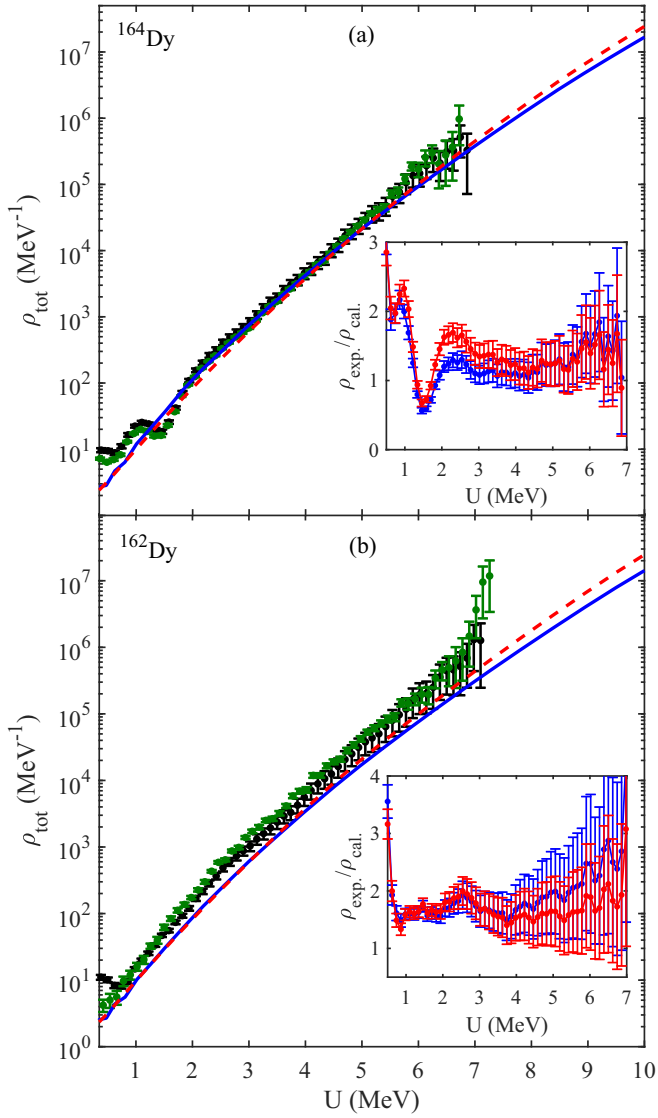

FIG. 10. Energy dependent total level densities with collective enhancements obtained using the macroscopic expressions (21) and (23) (red dashed line), and semiempirical calculations (26) (blue solid line) are compared with the corresponding experimental data (the green symbols are taken from Refs. [17,18] and the black symbols are taken from Ref. [19]) for ^{164}Dy and ^{162}Dy. The inserted panels show the ratio of the latest experimental data from Ref. [19] to the total level densities with collective enhancements obtained with macroscopic expressions (red line), and semiempirical calculations (blue line).

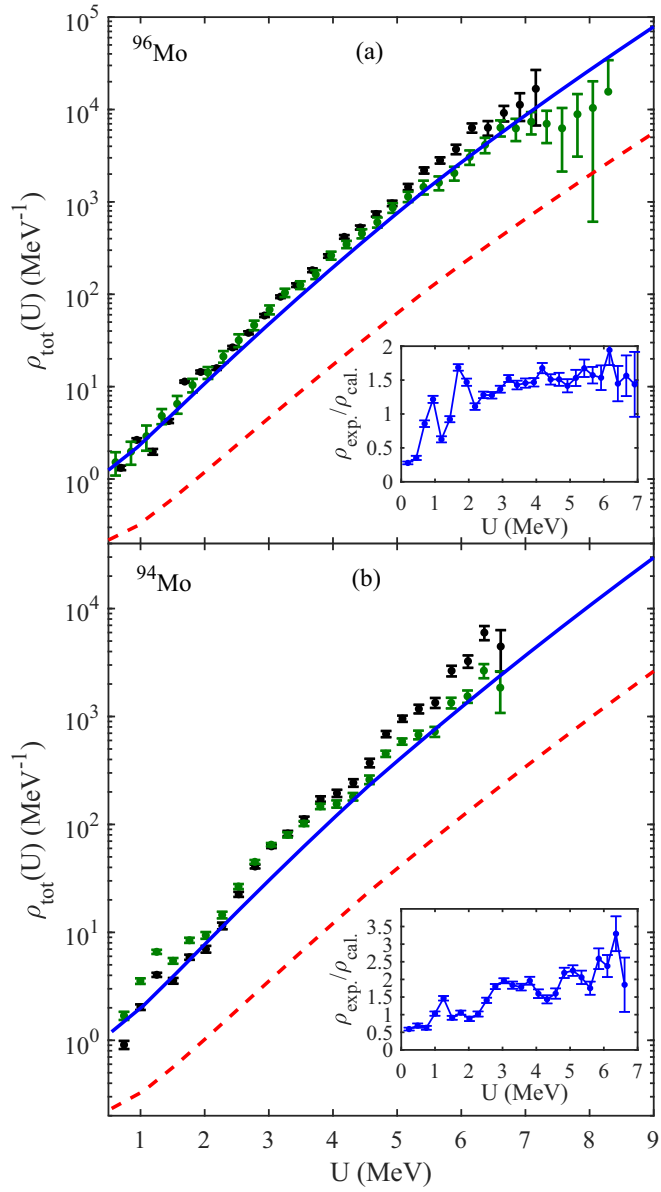

FIG. 11. Energy dependent total level densities with collective enhancements obtained with macroscopic expressions (21) and (23) (red dashed line), and in the semiempirical calculations (26) with spin dependent moment of inertia (blue solid line) are compared with the corresponding experimental data (the green symbols are taken from Ref. [20] and the black symbols are taken from Ref. [21]) for ^{96}Mo and ^{94}Mo. The inserted panels show the ratio of the latest experimental data from Ref. [21] to the total level densities obtained with the semiempirical collective enhancement.

factor from Eq. (26). Our calculations show that the total level density obtained in this way is almost the same as the one calculated with the general expression (16). The nuclear temperatures in the calculation of collective enhancements are obtained from Eq. (8) with the calculated level density parameters and excitation energies. The level densities obtained with the macroscopic expression for $K_{\rm coll}$ are also plotted. In the macroscopic calculations, the spin cut-off parameter is taken as from Eq. (13) assuming rigid-body moment of inertia ($\Im_{r.b.}$) and Eq. (12) is used in the microscopic calculations.

As seen in Fig. 10, both macroscopic and semiempirical calculations generally describe well the total level densities in ^{162}Dy and ^{164}Dy. An account of higher orders deformations in the semiempirical calculation of collective excitations is expected to improve the results at higher energies.

The comparison between the total level densities calculated with the macroscopic and semiempirical expressions for the collective enhancement and the corresponding experimental data [20,21] is shown in Fig. 11 for ^{94}Mo and ^{96}Mo. As seen,

assuming ^{94}Mo and ^{96}Mo as spherical isotopes, we fail to describe the experimental data. However, the spin dependent moment of inertia obtained with Eq. (18) in the microscopic calculation of vibration-rotational enhancement allows us to describe well the experiment. This implies that in the Mo isotopes with increasing excitation energy the shape changes from spherical to deformed and the nuclear system reverts to a rigid rotor with the rotational excitations. The same phenomenon is observed in σ^2/T curves of molybdenum isotopes presented in Sec. IV. Therefore, the use of the vibrational coefficient only is not enough to describe the energy dependent total level density in these isotopes. This observation is consistent with the analysis performed in Ref. [5].

VII. SUMMARY

The intrinsic level densities of well-deformed ^{160,162,164}Dy and almost spherical ^{94,96,98}Mo isotopes were calculated using the superfluid model with the single-particle energies taken from the QPM. The role of shell and pairing effects in the level density as well as their quenching with excitation energy are studied. The energy dependent level-density parameters, spin cut-off factors, and nuclear temperatures are calculated with the BCS model and their energy dependencies are studied. Collective effects are taken into account using the phenomenological macroscopic expression and semiempirical approach. Comparisons with the experimental level densities, show that both macroscopic and semiempirical approaches work well in Dy isotopes. However, the macroscopic approach with the assumption of an ideal spherical shape for Mo isotopes fails to describe the experimental data. In this case, a spin dependent moment of inertia was suggested based on the available experimental data of the yrast band. The semiempirical calculations with this moment of inertia are in a good agreement with the experiments. Despite the almost spherical equilibrium shape of Mo isotopes, the rotational enhancement should be taken into account. In ^{98}Mo, the Woods-Saxon single-particle spectra obtained in two minima (one spherical and another deformed) of the potential energy surface result in the close shell-correction values and in the intrinsic level densities. However, due to different dampings of shell and pairing effects, the ratio of the intrinsic level densities at deformed and spherical states is about 1.2–1.6 at low excitation energies.

ACKNOWLEDGMENT

This work was partly supported by the RFBR grants (17-52-12015 and 20-02-00176) and by Tomsk Polytechnic University Competitiveness Enhancement Program grant.

[1] S. Hilaire and S. Goriely, Nucl. Phys. A **779**, 63 (2006).
[2] S. Hilaire, J. P. Delaroche, and M. Girod, Eur. Phys. J. A **12**, 169 (2001).
[3] Y. Alhassid, G. F. Bertsch, S. Liu, and H. Nakada, Phys. Rev. Lett. **84**, 4313 (2000).
[4] Y. Alhassid, S. Liu, and H. Nakada, Phys. Rev. Lett. **99**, 162504 (2007).
[5] H. Uhrenholt, S. Åberg, A. Dobrowolski, Th. Døssing, T. Ichikawa, and P. Möller, Nucl. Phys. A **913**, 127 (2013).
[6] D. E. Ward, B. G. Carlsson, T. Døssing, P. Möller, J. Randrup, and S. Åberg, Phys. Rev. C **95**, 024618 (2017).
[7] H. Bethe, Rev. Mod. Phys. **9**, 69 (1937).
[8] A. S. Iljinov, M. V. Mebel, N. Bianchi, E. De Sancitis, C. Guaraldo, V. Lucherini, V. Muccifora, E. Polli, A. R. Re-olon, and P. Rossi, Nucl. Phys. A **543**, 517 (1992).
[9] T. von Egidy and D. Bucurescu, Phys. Rev. C **72**, 044311 (2005).
[10] P. D. W. Grochulski, A. Marinkowski, K. Siwek, and Z. Wilhelmi, Nucl. Phys. A **110**, 129 (1968).
[11] G. D. Adeev and P. A. Cherdantsev, Yad. Fiz. **21**, 491 (1975).
[12] A. N. Bezbakh, T. M. Shneidman, G. G. Adamian, and N. V. Antonenko, Eur. Phys. J. A **50**, 97 (2014).
[13] A. N. Bezbakh, T. M. Shneidman, G. G. Adamian, N. V. Antonenko, and S. G. Zhou, Eur. Phys. J. A **52**, 353 (2016).
[14] A. Schiller *et al.*, Nucl. Instrum. Methods Phys. Res. A **447**, 498 (2000).
[15] A. Schiller, M. Guttormsen, E. Melby, J. Rekstad, and S. Siem, Phys. Rev. C **61**, 044324 (2000).
[16] A. Schiller, A. Bjerve, M. Guttormsen, M. Hjorth-Jensen, F. Ingebretsen, E. Melby, S. Messelt, J. Rekstad, S. Siem, and S. W. Odegard, Phys. Rev. C **63**, 021306(R) (2001).
[17] M. Guttormsen, A. Bagheri, R. Chankova, J. Rekstad, S. Siem, A. Schiller, and A. Voinov, Phys. Rev. C **68**, 064306 (2003).
[18] H. T. Nyhus, S. Siem, M. Guttormsen, A. C. Larsen, A. Burger, N. U. H. Syed, H. K. Toft, G. M. Tveten, and A. Voinov, Phys. Rev. C **85**, 014323 (2012).
[19] T. Renstrøm, H. Utsunomiya, H. T. Nyhus, A. C. Larsen, M. Guttormsen, G. M. Tveten, D. M. Filipescu, I. Gheorghe, S. Goriely, S. Hilaire, Y. W. Lui, J. E. Midtbo, S. Peru, T. Shima, S. Siem, and O. Tesileanu, Phys. Rev. C **98**, 054310 (2018).
[20] R. Chankova *et al.*, Phys. Rev. C **73**, 034311 (2006).
[21] H. Utsunomiya *et al.*, Phys. Rev. C **88**, 015805 (2013).
[22] K. Heyde and J. L. Wood, Rev. Mod. Phys. **83**, 1467 (2011).
[23] T. Thomas *et al.*, Phys. Rev. C **88**, 044305 (2013).
[24] T. Thomas *et al.*, Nucl. Phys. A **947**, 203 (2016).
[25] K. Nomura, R. Rodriguez-Guzman, and L. M. Robledo, Phys. Rev. C **94**, 044314 (2016).
[26] A. B. Ignatyuk, *The Statistical Properties of the Excited Atomic Nuclei* (Energoatomizdat, Moscow, 1983).
[27] R. F. Casten and R. B. Cakirli, Phys. Scr. **91**, 033004 (2016).
[28] C. W. Reich, Nucl. Data Sheets **105**, 557 (2005).
[29] C. W. Reich, Nucl. Data Sheets **108**, 1807 (2007).
[30] B. Singh and J. Chen, Nucl. Data Sheets **147**, 1 (2018).
[31] D. Abriola and A. A. Sonzogni, Nucl. Data Sheets **107**, 2423 (2006).
[32] D. Abriola and and A. A. Sonzogni, Nucl. Data Sheets **109**, 2501 (2008).
[33] B. Singh and Z. Hu, Nucl. Data Sheets **98**, 335 (2003).
[34] T. Nikšić, Z. P. Li, D. Vretenar, L. Próchniak, J. Meng, and P. Ring, Phys. Rev. C **79**, 034303 (2009).
[35] Z.-H. Zhang, X.-T. He, J.-Y. Zeng, E.-G. Zhao, and S.-G. Zhou, Phys. Rev. C **85**, 014324 (2012).

[36] X. T. He and Z.-Z. Ren, Int. J. Mod. Phys. E **17**, 208 (2008).
[37] A.-C. Dai, F.-R. Xu, and W.-Y. Liang, Chin. Phys. C **43**, 084101 (2019).
[38] W. Y. Liang, C. F. Jiao, Q. Wu, X. M. Fu, and F. R. Xu, Phys. Rev. C **92**, 064325 (2015).
[39] A. N. Behkami and J. R. Huizenga, Nucl. Phys. A **217**, 78 (1973).
[40] A. L. Komov, L. A. Malov, and V. G. Soloviev, Izv. AN SSSR, Ser. Fiz. **35**, 1550 (1971).
[41] F. A. Gareev, S. P. Ivanova, L. A. Malov, and V. G. Soloviev, Nucl. Phys. A **171**, 134 (1971).
[42] W. Satula, J. Dobaczewski, and W. Nazarewicz, Phys. Rev. Lett. **81**, 3599 (1998).
[43] V. G. Soloviev, *Theory of Complex Nuclei* (Pergamon Press, Oxford, 1976).
[44] G. G. Adamian, N. V. Antonenko, S. N. Kuklin, B. N. Lu, L. A. Malov, and S.-G. Zhou, Phys. Rev. C **84**, 024324 (2011).
[45] G. G. Adamian, L. A. Malov, N. V. Antonenko, and R. V. Jolos, Phys. Rev. C **97**, 034308 (2018).
[46] M. Brack, J. Damgaard, A. S. Jensen, H. C. Pauli, V. M. Strutinsky, and C. Y. Wong, Rev. Mod. Phys. **44**, 320 (1972).
[47] P. Moller, A. J. Sierka, T. Ichikawab, and H. Sagawa, At. Data Nucl. Data Tables **109–110**, 1 (2016).
[48] H. A. Bethe, Phys. Rev. **50**, 332 (1936).
[49] Yu. V. Sobolev, *Level Densities of Atomic Nuclei* (Energoizdat, Moscow, 1990).
[50] A. B. Ignatyuk, G. N. Smirenkin, and A. S. Tishin, Yad. Fiz. **21**, 485 (1975).
[51] L. G. Moretto, Nucl. Phys. A **182**, 641 (1972).
[52] T. Ericson, Adv. Phys. **9**, 425 (1960).
[53] E. V. Mardyban, T. M. Shneidman, E. A. Kolganova, R. V. Jolos, and S.-G. Zhou, Chin. Phys. C **42**, 124104 (2018).
[54] G. Maino, A. Mengoni, and A. Ventura, Phys. Rev. C **42**, 988 (1990).